Composite Structures 212 (2019) 94–105

Contents lists available at ScienceDirect

Composite Structures

journal homepage: www.elsevier.com/locate/compstruct

# Analytical and experimental investigation on bond behavior of CFRP-to-stainless steel interface

Hongyuan Tang[a], Xuezhi Deng[a], Zhinbin Lin[b,*], Xiang Zhou[a]

[a] College of Architecture and Civil Engineering, Xihua University, Chengdu 610039, China
[b] Department of Civil and Environmental Engineering, North Dakota State University, Fargo, ND 58105, USA

ARTICLE INFO

*Keywords:*
CFRP sheets
Stainless steel
Bound-slip behavior
Elastic and plastic stages
Shear stress

ABSTRACT

Steel structures using stainless steel are recently accepted as more sustainable and durable systems. Although much research has been conducted on steel structures strengthened by carbon fiber-reinforcement polymer (CFRP) material, these steel structures are often made of conventional mild steel and thus existing prediction and analysis specified for mild steel cannot be directly extended for that of stainless steel. Therefore, this study aims to develop a new prediction model for determining the bond behavior of CFRP-to-stainless steel. Load time-history bond behavior was formulated in a piecewise manner to account for varying elastic, elastoplastic and debonding stages. A total of 22 stainless steel plates bonded with CFRP laminates were fabricated and tested to calibrate the model and further quantify the critical design parameters, including layers and anchorage length. Observation of the experiment showed that debonding failure between the adhesion layer and the CFRP sheets was dominant, partially suggesting the linear stress-strain relation for the CFRP and stainless steel. Comparison of results predicted by the proposed model to the test ones demonstrated that the proposed model has a high accuracy in prediction of bond stress and bond strength.

## 1. Introduction

In recent years, the stainless steel, due to its excellent ductility and superior resistance to corrosion, becomes emerging structural material as alternative for more sustainable and durable structures. Accordingly, some countries, including those in Europe and the United States, have developed the relevant design codes and specifications to the stainless steel [1–3]. Similar to the traditional mild steel, the stainless-steel structures could be strengthened and retrofitted by the use of the CFRP composite sheets that have been widely accepted as effective materials in civil engineering structures [4–9].

As identified [8,10–19], the selection and proper design of the CFRP composites to a structure are highly associated with the performance of the interfacial bond between the CFRP and steel substrate, that is, CFRP-to-steel interface. Literature review reveals that most studies either through experimental tests or analytical modeling have been conducted particularly on the bond behavior between the CFRP material and steel. From experimental standpoint [10–14], bond behavior was studied through the tests of adhesion strength of FRP to the mild steel components, for instance, Damatty and Abushagur [11] carried out the experiments involving shear lap testing of FRP sheets bonded to hollow steel sections to address the in-plane and out-of-plane behavior of the FRP sheets. Teng et al. [12] has presented an experimental study on the behavior of CFRP-to-steel bonded interfaces through testing of single-lap bonded joints. Nozaka [7] has analyzed and compared the stress distribution in the adhesive layer between a prototype repaired bridge girder and various specimens to determine an appropriate specimen and test setup for assessing the effective bond length of the adhesive. Zeng et al. [14] experimentally calibrated the mechanism of the debonding failure of CFRP strengthened H-section beams. Besides the mechanical properties, more recent studies have devoted to the long-term durability and various environmental conditions. Chandrathilaka et al. [15] presented their very recent study on bond behavior of the CFRP to steel under elevated temperature and discussed the impacts of the exposure of various temperature on bond curing. Yu et al. [16] reported the experimental study on long-term bond-slip behavior under coupled marine conditional and fatigue loading, and stated the bond reduction under laboratory accelerated durability tests. Other investigations [12,17–24] were carried out on the analytical modeling of nonlinear interfacial stress, bond-slip relation, and debonding behavior. Wu et al. [19] has studied two kinds of nonlinear constitutive laws and introduced the pre- and post-interfacial micro-debonding behavior, which enabled addressing nonlinear interfacial stress transfer and fracture propagation for different kinds of adhesive joints in FRP-

* Corresponding author.
*E-mail address:* zhibin.lin@ndsu.edu (Z. Lin).

https://doi.org/10.1016/j.compstruct.2019.01.007
Received 25 July 2018; Received in revised form 21 November 2018; Accepted 2 January 2019
Available online 06 January 2019
0263-8223/ 

strengthened steel structures. Teng et al. [12] has presented an analytical formulation for the entire load time-history bond behavior of CFRP-to-steel bonded joints with a ductile nonlinear adhesive based on a trapezoidal bond-slip model. By defining the trapezoidal bond-slip model, the interfacial-shear stress and load-displacement in different loading and debonding stages can be solved under the condition of sufficient adhesive thickness and bond length of the specimen. Moreover, Wang and Wu [18] recently explored the tri-linear bond-slip model for local bond behaivor of the CFRP-to-steel interface and derived the corresponding formulations to describe the debonding failure sequences. Clearly, despite these great efforts in the investigation of the steel structures strengthened by the CFRP material, these steel structures are often made of conventional mild steel. There is seldom study found in the literature to address the bond behavior between the CFRP and the stainless steel. As a result, the existing bond behavior prediction and analysis that are initially developed for mild steel will not fully account for that of stainless steel, due to inherent different surface and ductility of stainless steel. In addition, more laboratory or field experiments in terms of bond-slip relation or debonding failure modes could be an important supplementary for CFRP material applications in stainless steel structures.

Therefore, this study is to analytically and experimentally investigate the bond behavior of CFRP-to-stainless steel. Load time-history bond behavior is formulated in a piecewise manner to account for different pre- and post-debonding stages, including characteristics of bond-slip relation, and bond strength. The small-scale tensile bond tests are then conducted to calibrate the proposed model and verify the critical design parameters. Parametric study is finally carried out to better understand the critical factors and their impacts to the bond shear stress.

## 2. Formulation of bond behavior of CFRP-to-stainless steel

### 2.1. Basic assumptions

The CFRP-to-stainless steel failure [14,18] could occur: a) within the adhesive layer (cohesion failure) or b) adhesion failure between the steel and the adhesion layer, or c) adhesion failure between the CFRP sheets and the adhesion layer, as well as FRP sheet rupture. The adhesion bond strength depends much on the choice of component material, the method and degree of surface treatment [10–19]. For a linear adhesive, the bond-slip curve was shown to have an approximately bilinear shape which is similar to that of CFRP-to-concrete bonded joints. According to the experiment of CFRP-concrete interface, Xia and Teng [20] has carried out a series of tensile tests on CFRP-steel interface, and has put forward a bilinear bond-slip model of CFRP-steel interface, as shown in Fig. 1. On the basis of the research of Xia model, through the experiment and finite element analysis, Fawzia et al. [21]

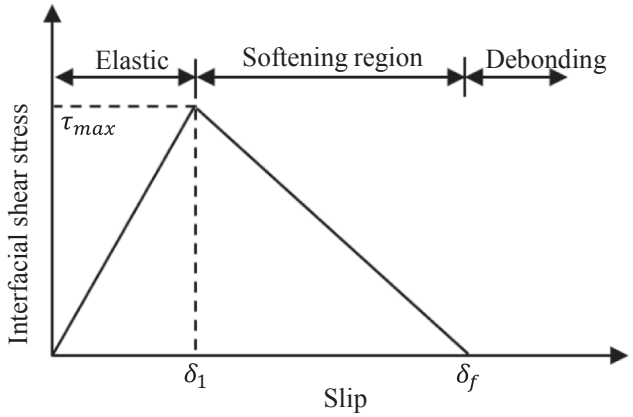


**Fig. 1.** Bond-slip curves for linear adhesives [20].

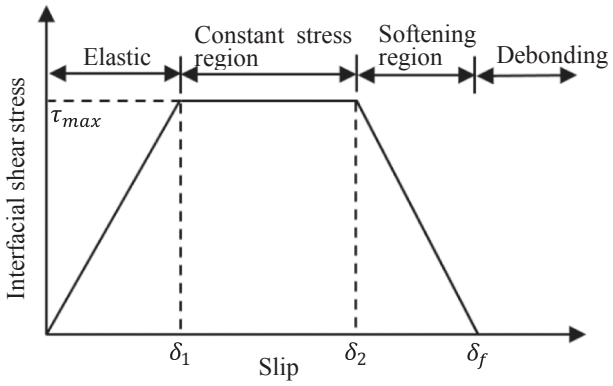


**Fig. 2.** Bond-slip curves for nonlinear adhesives [12].

has studied the influence of the adhesive thickness on the model slip, and corrected the adhesive thickness of the bilinear bond-slip model. Compared with linear adhesives, the nonlinear adhesives has better ductility, larger strain capacity and higher tensile strength. In order to study the interfacial bonding strength between CFRP and steel, Teng et al. [12] has proposed a trapezoidal bond-slip model for nonlinear adhesive, and analyzed the whole process of bonding and debonding, as shown in Fig. 2.

A full-range load-displacement curve is schematically developed for describing the CFRP-to-steel bonded joints with a nonlinear ductile adhesive, as shown in Fig. 3, where the debonding only occurs once in the process of failure, and the interface failure is within the adhesive layer (i.e., cohesion failure). This concept is due to the fact that stainless steel exhibits different mechanical properties, including its roughness after surface treatment, as compared to the traditional mild steel. As a result, the requirements of the adhesion in terms of thickness between the CFRP sheets and steel plate and the corresponding bond behavior could lead to different debonding failure modes against the conventional observation for mild steel in the previous studies [8,10–19]. Therefore, the proposed load-elongation curve, shown in Fig. 3, was revised from the previous work by Yuan et al. [25] to account for the high nonlinearity experience in interfacial bonding shear force due to the stainless steel material. The shear stress of the adhesion remains intact after the yield stress. When the debonding load is reached, the first debonding occurs. There was no obvious descending section, and the interface failure occurs at the adhesion failure between the adhesion and the CFRP. Consequently, there was a sudden drop in shear load. The final failure was followed up by several times debonding.

According to the literature review, the stress-strain relationship of CFRP sheets could be defined in a linear manner as shown in Fig. 4(a), while Fig. 4(b) is plotted for the simplified shear stress-strain relationship of the binder with an ideal elastic-plastic behavior, where

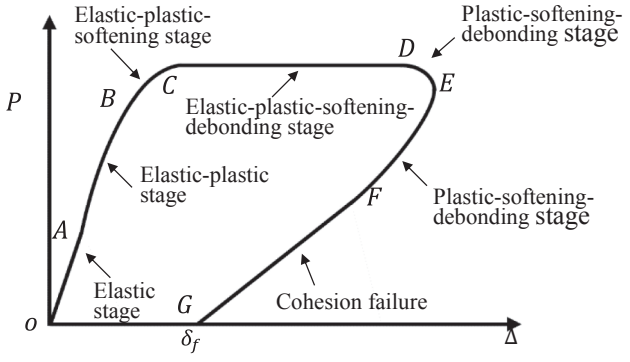


**Fig. 3.** Defined Load time-history bond-slip curve for CFRP-to-steel bonded joints with a nonlinear ductile adhesive (replotted and revised from [25]).

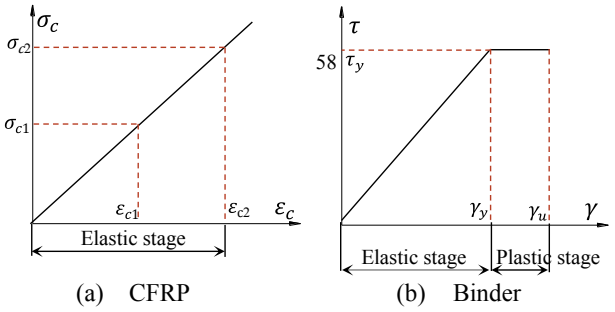


**Fig. 4.** Simplified stress-strain curves of CFRP and binders.

$\gamma_y$and $\gamma_u$ are yielding and ultimate shear strain and can be determined based on experimental testing.

To simplify the analysis, the following assumptions are made:

- o The adhesive layer can be regarded as the shearing spring, and it only bears the shear stress $\tau$, ignoring the transverse stress (debonding stress).
- o In the range with CFRP sheet bonded, the adhesive layer is isotropic, and the thickness of adhesive layer is even, so the shear stress at the same position is unchanged along the thickness direction.
- o The adhesive layer is regarded as the ideal elastic-plastic material, and the stress of CFRP and stainless steel plate is in the range of elastic stage, regardless of plasticity development.
- o During the test, the composite specimen is in one-way force state, and the additional bending moment caused by eccentrically loading can be ignored.

### 2.2. Force analysis of composite members

Consider a composite with force equilibrium among stainless steel, CFRP sheet and adhesion layer, per unit length $dx$ for any point $x$. Due to the working condition of uniaxial stresses, the CFRP-to-adhesive and adhesive-to-stainless steel plate interfaces were simplified as a model of shear stress, as shown in Figs. 5 and 6. According to the previous works [18,26–28], the whole process from the beginning of loading to the first debonding of CFRP sheets was analyzed.

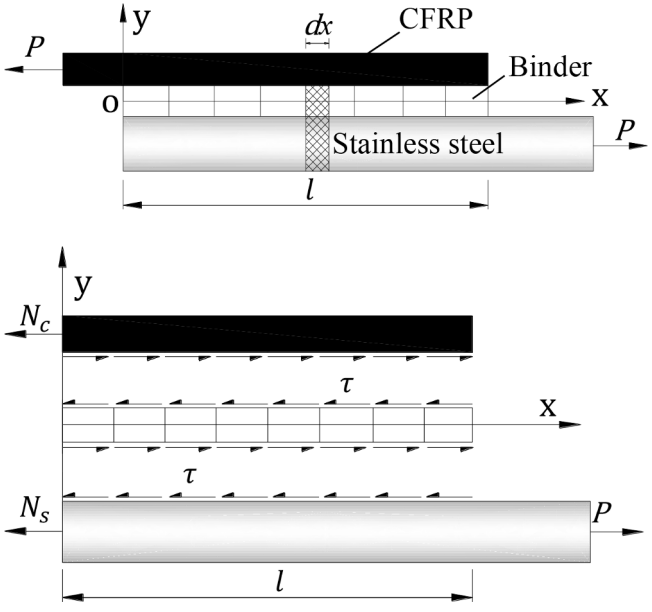


**Fig. 5.** Mechanical model of composite specimen.

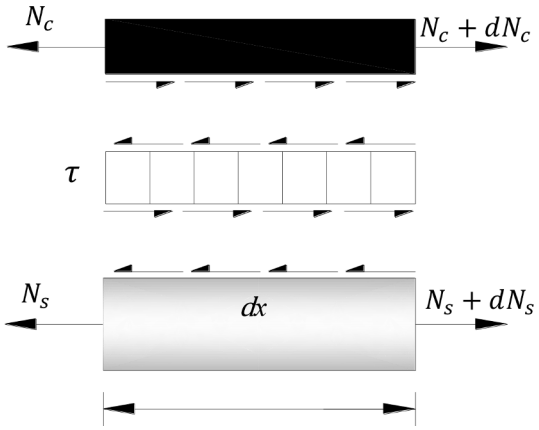


**Fig. 6.** Stress model of micro-element.

When the specimen was in the elastic stage, the shear stress of the adhesive layer increased with the increasing of the external force ($P$). When the maximum shear stress of the adhesive layer had just reached the yield stress ($\tau_y$), the adhesive layer entered into a plastic stage, and the zone distributed with shear stress expanded to the place of $l_e$ far from the seam. At this moment, the shear stress zone at the elastic stage achieved the maximum. And the adhesive layer was still in an elastic stage in the zone ($0 \le x < l_e$). As the external force ($P$) continued to increase, one part of the shear stress in the adhesive layer came into a plastic stage gradually. But there was still elastic zone far from the seam. When the plastic zone expanded to the maximum ($0 \le x < l_p$), the elastic zone would fully develop to the end of the CFRP sheet. At this time, the zone ($0 \le x < l_p$) was a plastic zone, but the area ($l_p \le x \le l_p + l_e$) was still an elastic area. And the plastic and elastic zone above mentioned were namely called effective bonding length ($l = l_e + l_p$).

$P$ is the external load. $N_s$ and $N_c$ are the force of stainless steel plate and CFRP sheets, respectively. The section area of stainless steel plate and CFRP sheets are $A_s$ and$A_c$, respectively. The displacements of stainless steel plate and CFRP sheets are $u_s$ and $u_c$, respectively. And their tensile stresses are $\sigma_s$ and $\sigma_c$, respectively. $E_S$, $E_C$ and $G_a$ are the elastic modulus of stainless steel, CFRP sheets and the shearing modulus of the adhesive layer, respectively.

According to Fig. 5, the static equilibrium conditions can be obtained as

$$P = N_s + N_c = \sigma_s A_s + \sigma_c A_c \tag{1}$$

Also, according to Fig. 6, the force balance of the element $dx$ can be achieved as Eq. (2)

$$\frac{d\sigma_s}{dx} = \frac{b_c \tau}{A_s}, \quad \frac{d\sigma_c}{dx} = -\frac{\tau}{t_c} \tag{2}$$

The geometrical equation and Hooke's Law can be given by Eq. (3) as follows,

$$\varepsilon_s = \frac{du_s}{dx}, \quad \varepsilon_c = \frac{du_c}{dx}, \quad \sigma_s = E_S \varepsilon_s, \quad \sigma_c = E_C \varepsilon_c, \quad \tau = G_a \gamma_e \tag{3}$$

According to the slip ($u_s - u_c$) between the CFRP and the stainless steel, the adhesive layer has uniform shear stress ($\tau$) and strain ($\gamma$) along the thickness direction. And the shear strain can be given by,

$$\gamma = \frac{u_s - u_c}{t_a} \tag{4}$$

According to the boundary conditions: when $x=0$, $\gamma=\gamma_y$; when $x=l_p$, $N_s=0$; $N_s$ and $N_c$ are continuous in the elastic stage ($x=l_e$) and the plastic stage ($x=0$).

Only the derivation results were herein listed. The whole shear strain distribution rule of the adhesive layer in elastic-plastic stages are

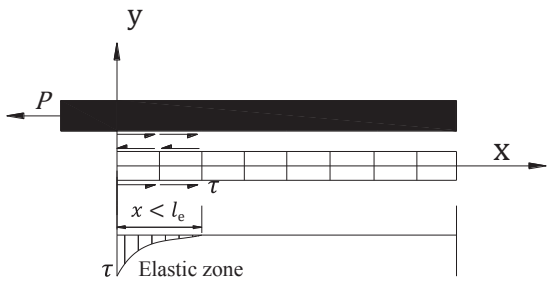


(a) Initial elastic stage

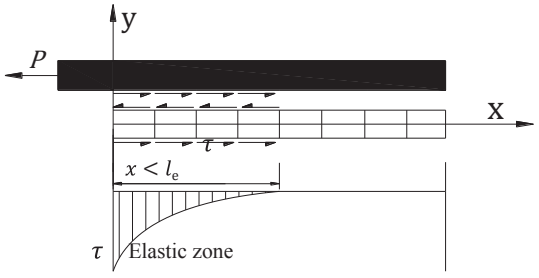


(b) Yield point of shear stress in the adhesive layer

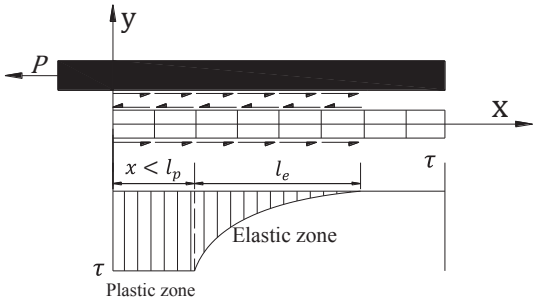


(c) Elastic-plastic stage

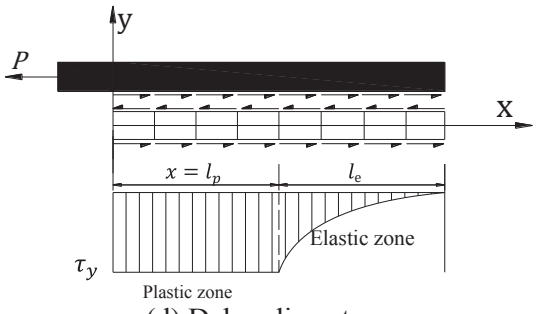


(d) Debonding stage

**Fig. 7.** Shear Stress distribution associated to bond.

given in the form as shown below.

(1) When the shear load $P \le \beta\gamma_y t_a E_C A_C$, the adhesive layer only appears elastic zone, as shown in Fig. 12. At this point, the shear strain distribution can be shown by,

$$\gamma_e(x)=\frac{PG_a}{\beta t_a E_C A_C sinh(\beta l)}\sinh[\beta(l-x)], \quad 0 \le x \le l \tag{5}$$

(2) When the adhesive layer just goes into the plastic stage, that is $l_p = 0$, as shown in Fig. 14. At this moment, the critical load can be given by,

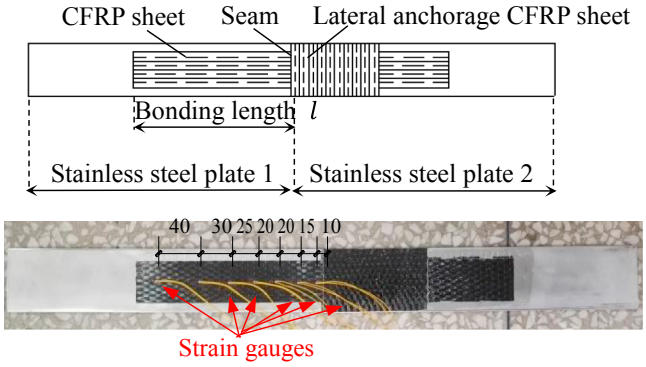


**Fig. 8.** Instrumented specimens.

$$P_y=\beta\gamma_y t_a E_C A_C \tag{6}$$

(3) When the shear load $P > \beta\gamma_y t_a E_C A_C$, the plastic zone appears in the adhesive layer, as shown in Fig. 16. At this moment, the shear strain distribution can be given by,

$$\gamma_e(x_1)=\frac{\gamma_y}{sinh(\beta l_e)}sinh[\beta(l_p+l_e-x_1)], \quad l_p \le x_1 \le l_p+l_e \tag{7}$$

$$\gamma_p(x_2)=\frac{\beta^2}{2}\gamma_y(l_p-x_2)^2+\beta\gamma_y(l_p-x_2)+\gamma_y, \quad 0 < x_2 \leqslant l_p \tag{8}$$

The above mentioned $\beta$ is a correction coefficient of the adhesive layer. It can be given by Eq. (9) with the unit of $mm^{-1}$.

$$\beta^2=\frac{G_a}{t_a}\left(\frac{1}{E_s}\frac{b_c}{A_s}+\frac{1}{E_c t_c}\right) \tag{9}$$

### 2.3. Derivation of bond-slip relation

Inspired by early work from Teng et al. [12], the bond-slip relation could be described as different stages, as shown in Fig. 7.

(a) Initial elastic stage
In the early stages of loading, the composite member was in the elastic stage, as shown in Fig. 7(a). The shear strain of CFRP sheets was mainly concentrated in the zone near the seam end ($x < l_e$), and there was very little shear strain existing in the area far from the seam end. Meanwhile, the strain of CFRP sheet was synchronized with the strain development of the adhesive layer. The tensile stress ($\sigma_c$) of the CFRP sheet and the shear stress ($\tau$) of the adhesive layer increased linearly with the strain growth. And the elongation increased with the external shear load. The external load ($P$) can be obtained by.

$$P=\int_0^x \tau_e(x)dx=\frac{G_a\gamma_y}{\beta sinh(\beta l_e)}[cosh(\beta x)-1], \quad 0 \le x < l_e \tag{10}$$

(b) Beginning yield of shear stress in the adhesive layer
The specimen began to enter into the elastic-plastic stage, as shown in Fig. 7(b). At this time, the distribution of shear stress of CFRP sheets developed to the widest range ($x = l_e$), and the shear stress at the seam end began to yield. Hereafter, the shear strain ($\varepsilon_c$) of CFRP sheet was no longer synchronized with the shear strain ($\gamma$) development of the adhesive layer. Meanwhile, the tensile stress ($\sigma_c$) at the CFRP sheet was far below the yield strength and continue increasing. However, the shear stress of the adhesive layer had reached the yield stress ($\tau_y$). At this time, there was a critical load given by.

$$P_y=\beta\gamma_y t_a E_C A_C \tag{11}$$

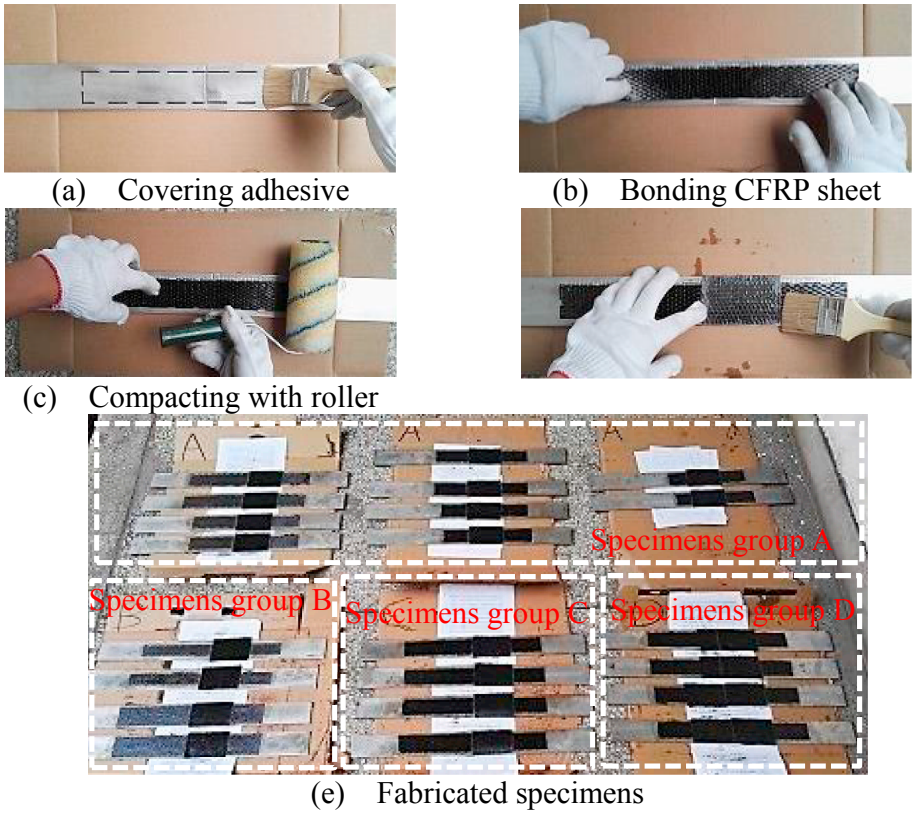


**Fig. 9.** Fabrication process of specimens.

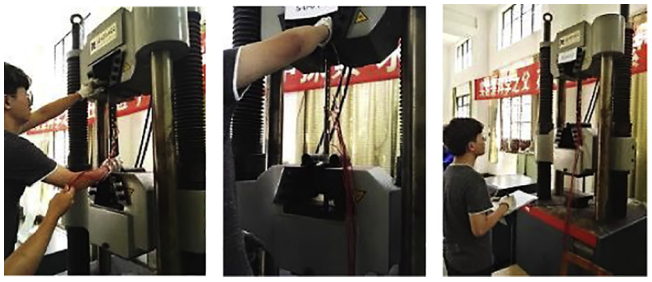

**Fig. 10.** Sample testing.

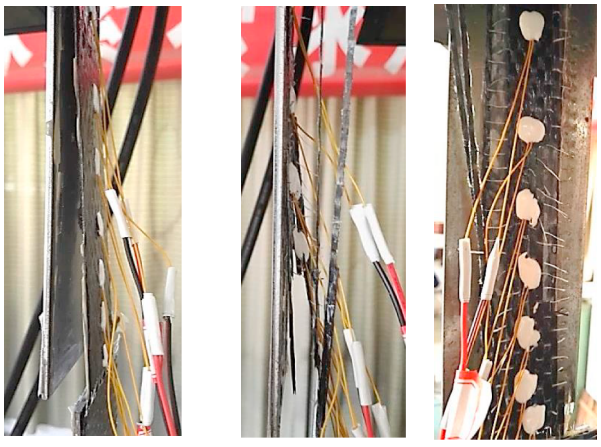

(a) Completely debonding failure (b) Splitting failure

**Fig. 11.** Failure modes of debonding.

(c) The elastic-plastic stage

In the plastic stage, the area ($x < l_p$) was a plastic zone near the seam end, and the elastic zone ($l_p < x < l_p + l_e$) gradually developed to the area farther away from the seam end, as shown in Fig. 7(c), at this time, the external load $P$ can be given by.

$$P = \int_0^{l_e} \tau_e(x)dx + \tau_y \bullet x \tag{12}$$

$$P = P_y + \tau_y x = \beta\gamma_y t_a E_C A_C + \tau_y x \tag{13}$$

In the plastic phase, the curve had an approximate level of yielding platform, as shown in Fig. 7(c). From the Eq. (11), the shear force ($P_y$) of the elastic zone was a constant. The shear stress ($\tau$) reached the yield shear stress ($\tau_y$) and no longer increased. The whole test adopted a displacement control, and the $\Delta x$ in a unit time was a constant. Therefore, the shearing resistant force ($N_a = P_y + \tau_y x$) of the adhesive layer had little change in a linear manner, as shown in Fig. 7(c). This phase lasted for a very short time. It was mainly due to the bonding effect between the CFRP sheet and adhesive layer, and the increase of tensile stress ($\sigma_c$) in CFRP sheets was affected, which led to the slow increase in the internal resistant force ($N_c + N_s$) of composite specimen.

With the development of plastic zone, the bonding effect of CFRP-adhesive layer decreased gradually, and the strain ($\varepsilon_c$) of CFRP sheets increased faster than the strain ($\gamma$) of adhesive layer. The adhesive layer gradually withdrew from the resistance to shear load. The elastic modulus($E_c$) of CFRP sheet is much greater than the elastic modulus ($E_a$) of adhesive layer, and thestress($\sigma_c$) changed quickly. Meanwhile, the positive stress of the composite specimen increased and the curve turned into a sudden upward trend, as shown in Fig. 7(c). The bonding effect between the CFRP and adhesive layer tended to “collapse”, but no debonding occurred.

(a) Interface damage of completely debonding (b) Interface damage of mixed damage

**Fig. 12.** Failure mode of bonding interface.

(d) The debonding stage

The plastic zone near the seam end reached the maximum range ($x = l_p$), and the elastic zone expanded beyond the seam end, as shown in Fig. 7(d). The entire bonding length achieved the maximum ($l = l_e + l_p$), and the strain of adhesive layer in the plastic zone reached the extreme value($\gamma_u$). The adhesive layer cannot continue to resist the external shear load, and the first debonding occurred. The shear load reached the debonding load ($P_d$) which can be calculated by.

$$P_d = P_y + \tau_y l_p \tag{14}$$

## 3. Experimental test and calibration

To calibrate the proposed model above and determine critical factors, such as the length, width, number of layers of the bonded CFRP sheets, and also the anchorage length of CFRP sheet, a total of 22 specimens as four groups were tested in the laboratory, as shown in Table 1, where $l$ indicates the length of CFRP sheet; $b_c$ indicates the width of CFRP sheet; $n$ indicates the number of CFRP sheet layers; $l_a$ indicates the length of the extra transvers CFRP sheet. Specimen s-0-0 is labelled as the specimen with CFRP sheets of 180-mm bonding length. Specimens S-A-1/S-A-4 were used to study the effect of bonding length of CFRP sheets on bonding properties. Specimens S-B-1/S-B-2 were used to study the effect of bonding width of CFRP sheets on bonding properties, Specimens S-C-1/S-C-2 for layers of CFRP sheets and Specimens S-D-1/S-D-2 for anchorage length of CFRP sheets. The specific parameters of the test components are described in detail in the following sections.

### 3.1. Test specimens

The cleanliness and roughness of the surface of stainless steel plate have a significant effect on the bonding behavior of the binder. Before the experiment, the roughness of the surface of stainless steel plate was polished with a steel wire wheel, and the surface roughness could be increased to improve the mechanical biting force between the base material and the adhesive layer, thus enhancing the bonding ability. Afterwards, the polished stainless steel plate was carefully cleaned with a brush, and then the stainless steel plate and CFRP sheets surface were wiped with the degreased cotton cloth soaked with anhydrous alcohol, so as to remove the dust, greasy dirt and other stains on the surface. Finally it was dried for use.

The specimen is composed of two austenitic stainless steel plates with externally bonded CFRP sheets on the same side. The thickness of two stainless steel plates are 3 mm and closely stitched. In order to test the strain of CFRP sheets under shear load, some strain gauges were bonded on the CFRP sheets at certain distance along the longitude. Meanwhile, to ensure that the damage of CFRP sheets occurred on the side of stainless steel plate, two layers of extra CFRP sheets were transversely bonded on the side of stainless steel plate 2 near the seam of 100 mm, as shown in Fig. 8. The fabrication process of specimens is shown in Fig. 9.

### 3.2. Material properties

The CFRP sheet used is of MH-300 type and the adhesive was produced by Carbon Composite Material Co. Ltd. in China. The stainless steel plate was made by Panzhihua Steel Co. Ltd. in China. The mechanical properties and material parameters of each kind material used are shown in Tables 2–4, where $c$ indicates the physical quantity of the CFRP sheet. $a$ indicates the physical quantity of the adhesive layer. $s$ indicates the physical quantity of stainless steel. $t$ is the material thickness. $b$ is the width of CFRP sheet. $\delta$ is elongation. $\sigma_c$ is the ultimate strength of CFRP. $\upsilon_a$ is the Poisson ratio of adhesive layer. $\sigma_a$ is the ultimate strength of adhesive layer. $\sigma_{s1}$ is the yield strength of stainless steel and $\sigma_{s2}$ is the ultimate strength of stainless steel.

### 3.3. Test setup and instrumentation

As shown in Fig. 10, the samples were loaded by an electrohydraulic servo universal test machine of css-waw1000 type. A displacement control mode was performed and the loading rate is controlled at a speed of 0.5 mm/min. The instrumentation was plotted in Fig. 8, where the strain gauges were embedded and distributed within the adhesion layers. The strain gauges data were collected by a programmable static strain meter of YE2533 type. In order to study the possible effect factors, the main parameters in the test are the varying width of CFRP sheet, the CFRP layer number, the bonding length of CFRP sheet and the length of extra transvers CFRP sheet as an anchorage of the CFRP sheets tested. The emphasis was focused on the shear yield load, debonding load, ultimate load and tensile strain of CFRP-stainless steel plate composite members. During the loading process, the debonding development of CFRP sheets and the damage of the components were carefully recorded.

## 4. Test results and discussions

### 4.1. Failure modes

The debonding failure between the CFRP sheet and the stainless steel plate occurred in all specimens. And the debonding failure included two kinds of failure modes, completely debonding failure and splitting failure in the test. The failure process is roughly as follows. As the adhesive is the weak part of the stainless steel plate strengthened with CFRP sheet, a slightly debonding failure firstly occurred at the adhesive when the load reaches about 50% of the ultimate load. With the increasing of load, the debonding range rapidly extended from the seam to the distance. Finally, the bonding failure between CFRP and adhesion leads to completely debonding between CFRP sheets and stainless steel plate, as shown in Fig. 11.

However, due to the fabrication deficiency, the adhesive in a few specimens cannot completely saturate the CFRP sheets, which resulted that the fiber bundles of CFRP sheets unable to form a whole composite member to bear the shearing load. This fabrication deficiency caused a few specimens occurred splitting failure mode between the CFRP sheets and stainless steel plates instead, as shown in Fig. 11(b).

When the bonding length ($l$) between CFRP sheets and stainless steel plate is no more than 75 mm, the failure mode of CFRP-stainless steel plate interface is a completely debonding of adhesive-stainless steel plate interface. In this failure mode, the adhesive layer completely debonded from the stainless steel plate, and the surface of stainless steel

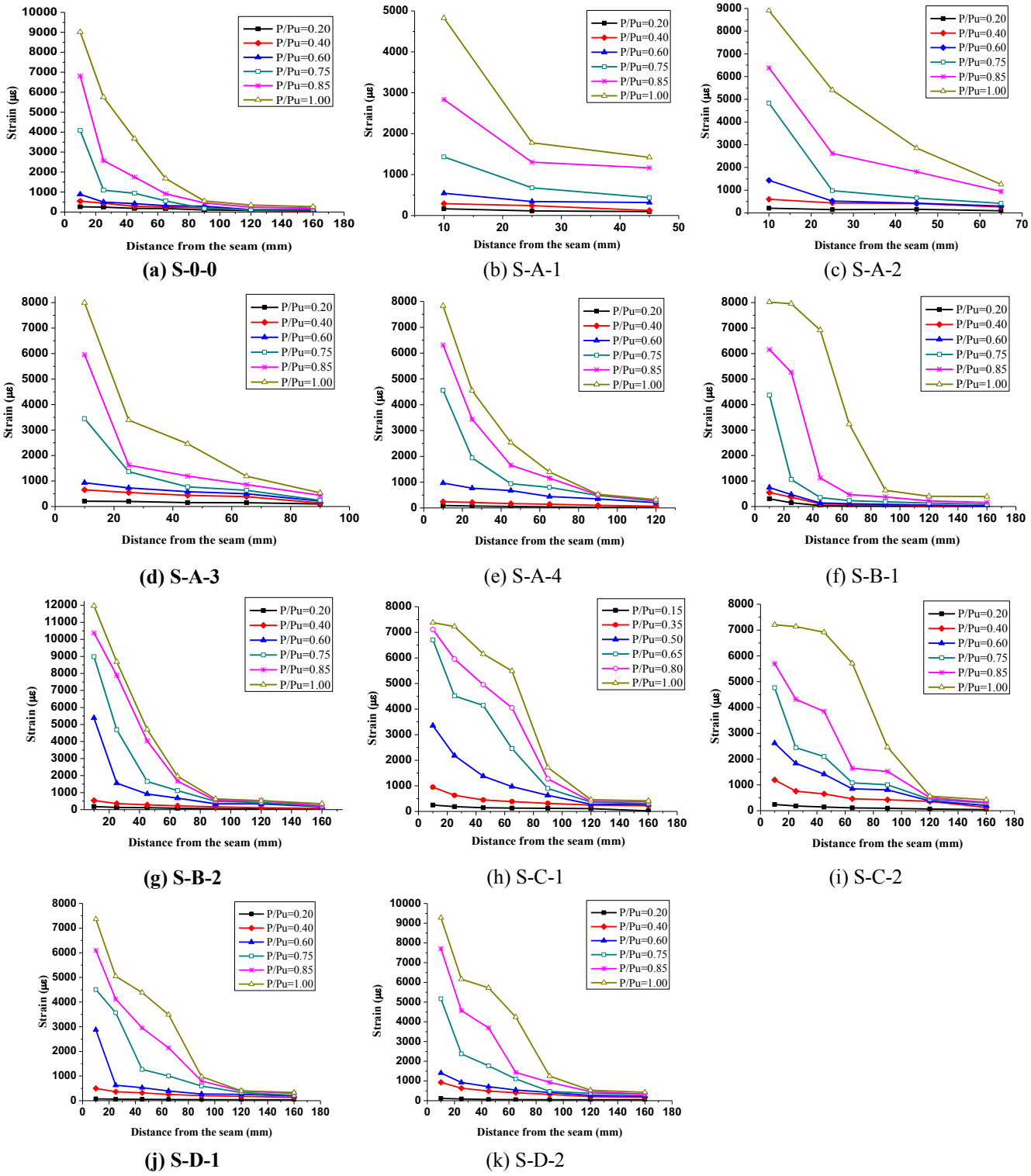


**Fig. 13.** The strain distribution curves of CFRP sheets in parts specimens.

plate is smooth, without adhesive layer residue, as shown in Fig. 12(a). When the bonding length ($l$) between CFRP sheets and stainless steel plate is more than 75 mm, the failure mode of CFRP-stainless steel plate interface is a mixed failure. In this failure mode, the adhesive layer completely debonded from the stainless steel plate near the seam. However, far away from the seam, the damage occurred in the adhesive layer and some of the adhesive and fiber residues stayed on the surface of the stainless steel plate, as shown in Fig. 12(b).

### 4.2. Shear stress of CFRP sheets

The strain distribution curve of CFRP sheets bonded on the stainless steel plate involved six loading situations, $0.2P_u$, $0.4P_u$, $0.6P_u$, $0.75P_u$, $0.8P_u$ and $P_u$, as shown in Fig. 13. The strain curves of these loading situations of reflected the process of strain changes during the whole loading process.

It can be seen from Fig. 13 that the strain of the whole CFRP sheets was smaller at the initial stage of loading. With the increasing of

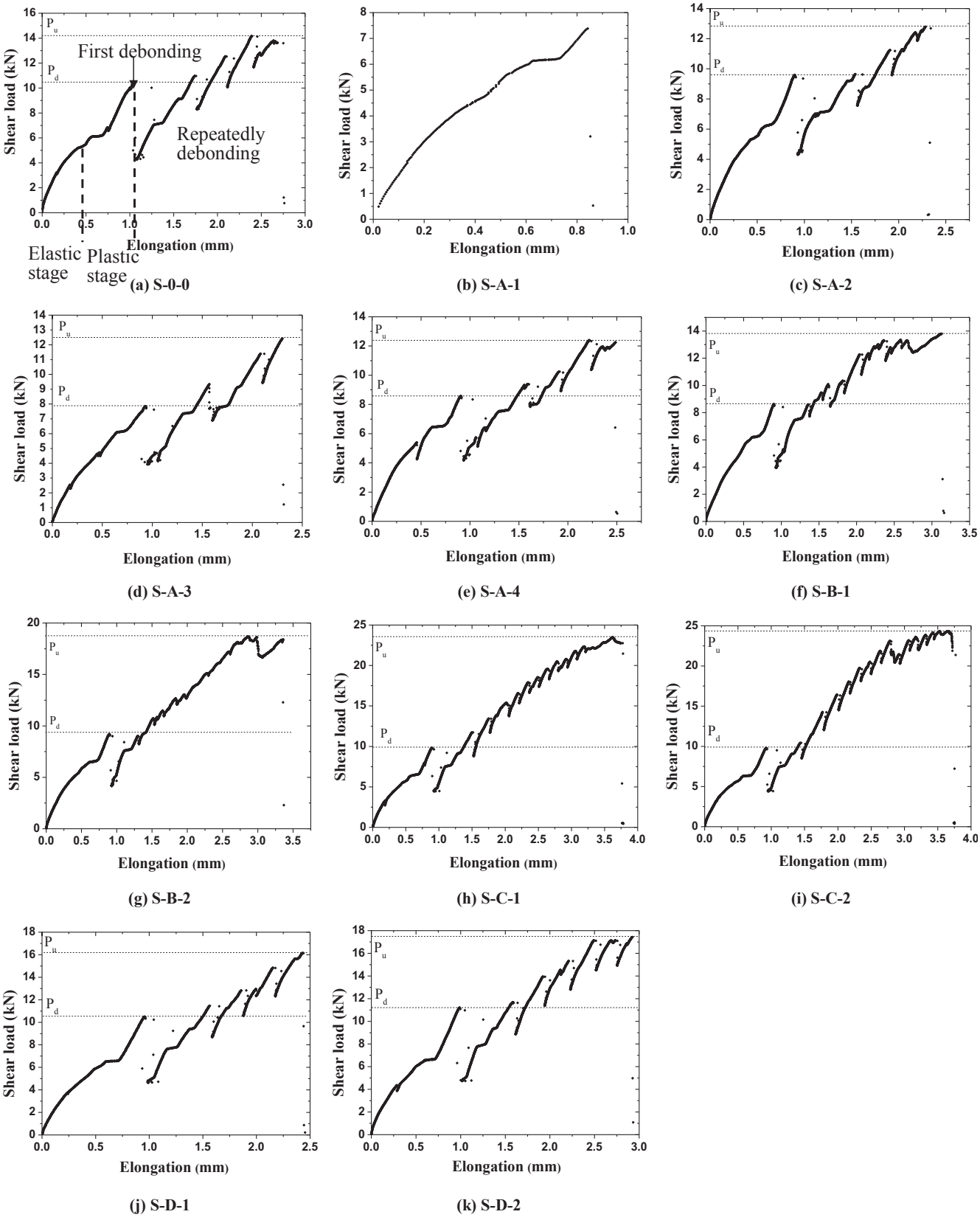


**Fig. 14.** Shear load-elongation curves of the CFRP samples.

loading, the strain of CFRP sheets near the seam increased significantly, but the strain far away from the seam was still small. When the load reached 60% of the ultimate bonding capacity, the shear stress at the bonding interface was mainly distributed in the area within 25 mm of the seam. When the load reached 85% of the ultimate bonding capacity, the shear stress mainly concentrated in the range of 65 mm from the seam. As the loading closed to the ultimate bonding capacity, the shear stress at the bonding interface expanded to the range of 100 mm from

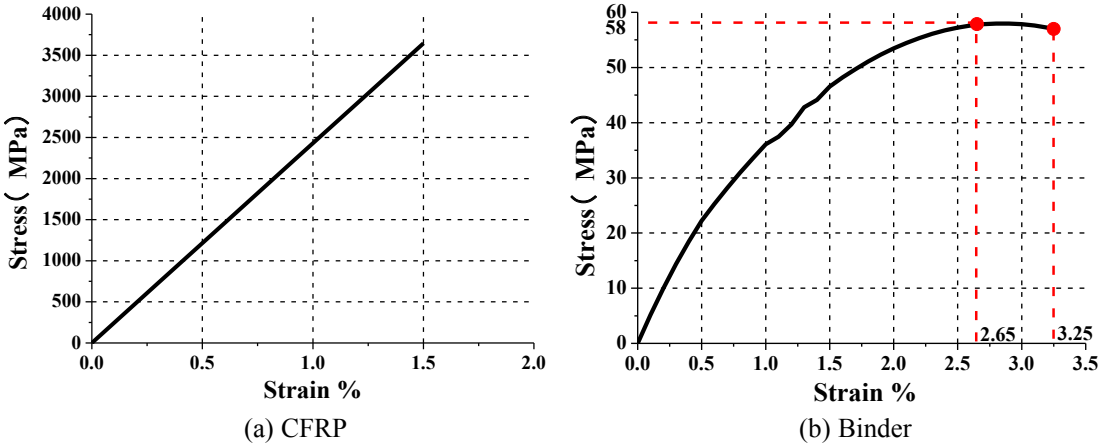


**Fig. 15.** Stress-strain curves of CFRP and binder.

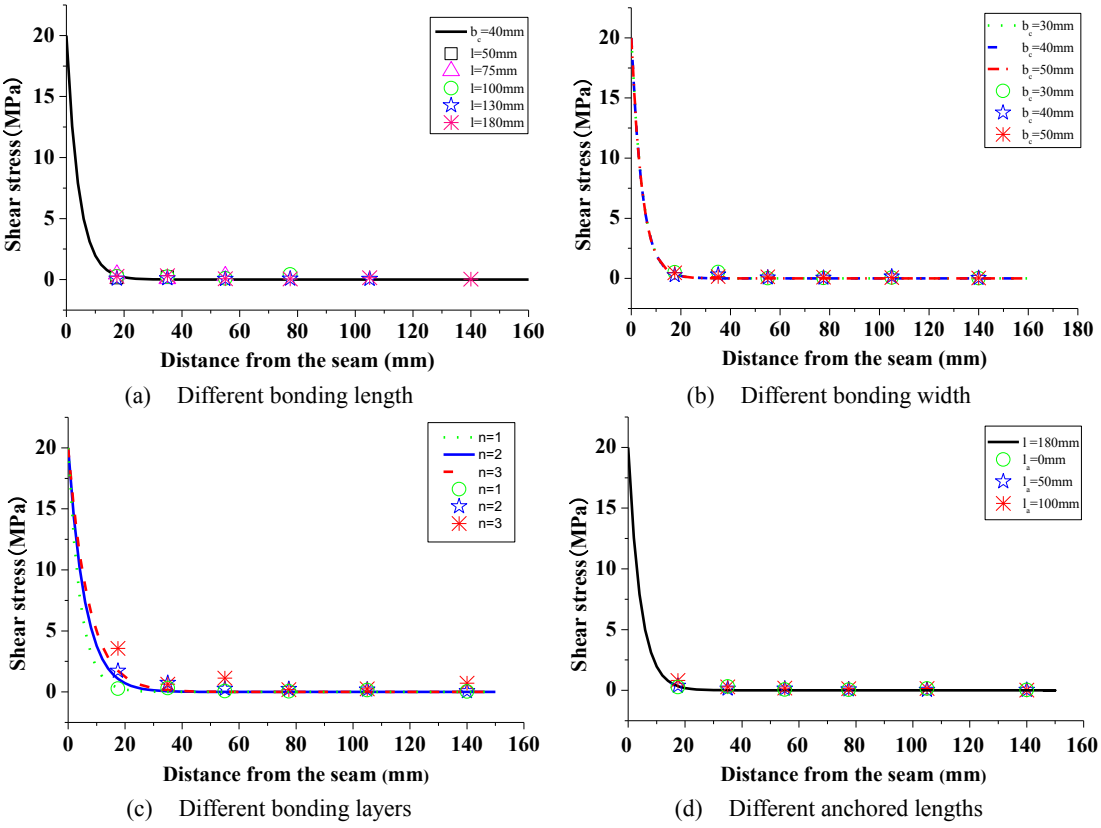


**Fig. 16.** Shear stress distribution between CFRP and steel plates in elastic phase.

the seam, and only a small part of shear flow existed in the area exceeding 120 mm from the seam. This phenomenon indicated there was an effective bonding length, that is, the CFRP sheets in this effective bonding length withstand most part of the shear load.

By analyzing the strain distributions and test results of different specimens, it was found that the length and width of CFRP sheets had little effect on the effective bonding length of CFRP sheet. However, increasing the number of CFRP sheet layer and the length of extra transverse CFRP sheets can improve the effective bonding length. With the increasing of bonding length and width of CFRP sheet, the number of CFRP sheet layers and the length of extra transverse CFRP sheets, while the ultimate bonding capacity of CFRP sheets improved in different degrees, but these factors had little influence on the yield load and debonding load.

### 4.3. Load-elongation curve of CFRP sheets

The shear load-elongation curve of the CFRP sheets directly reflected the behavior of the stainless steel plate reinforced with CFRP sheets, especially the slippage and debonding of the CFRP-stainless steel plate interface during the whole tensile process. The shear load-elongation curve of specimens were shown in Fig. 14, and the critical/ultimate capacity of shear load of each specimen as shown in Table 5.

Fig. 14 displayed the shear-elongation curves, where loading drops responded for the debonding of CFRP sheets. The shear stress of the adhesion remains unchanged after reaching the yield stress, as illustrated in Fig. 14(a). The first debonding fracture happened when the load passed the yield stress, with a corresponding sudden drop. The load bumped back before reaching another debonding fracture. Clearly, the most samples experienced similar trend with a wave-shaped

**Table 1**
Tested matrix of the samples.

| Group | Specimen number | $l$/mm | $b_c$/mm | $n$/layer | $l_a$/mm |
|---|---|---|---|---|---|
| A | S-0-0 | 180 | 40 | 1 | 0 |
| | S-A-1 | 50 | | | |
| | S-A-2 | 75 | | | |
| | S-A-3 | 100 | | | |
| | S-A-4 | 130 | | | |
| B | S-B-1 | 180 | 30 | 1 | 0 |
| | S-B-2 | | 50 | | |
| C | S-C-1 | 180 | 40 | 2 | 0 |
| | S-C-2 | | | 3 | |
| D | S-D-1 | 180 | 40 | 1 | 50 |
| | S-D-2 | | | | 100 |

**Table 2**
Parameters of CFRP sheet.

| $t_c$/mm | $b_c$/mm | $E_c$/MPa | $\sigma_c$/MPa | $\delta_c$/% |
|---|---|---|---|---|
| 0.167 | 30 | $2.43 \times 10^5$ | 3418 | 1.71 |

**Table 3**
Parameters of adhesive.

| $t_a$/mm | $b_a$/mm | $E_a$/MPa | $\upsilon_a$ | $\sigma_a$/MPa | $\delta_a$/% | $\gamma_u$ |
|---|---|---|---|---|---|---|
| 0.5 | 30 | 2584 | 0.35 | 58 | 3.25 | 0.0325 |

**Table 4**
Parameters of stainless steel plate.

| $t_s$/mm | $b_s$/mm | $E_s$/MPa | $\sigma_{s1}$/MPa | $\sigma_{s2}$/MPa | $\delta_s$/% |
|---|---|---|---|---|---|
| 3 | 60 | $1.96 \times 10^5$ | 273 | 621 | 60 |

fluctuation in accordance with energy release due to the debonding fracture, as shown in Fig. 14(a)–(k). The results of Category A confirmed that the elongation increased as expected, with the increase of the bonding length. Also the test samples with the larger width (of bonding areas) achieved the higher bonding capacity and slightly higher elongation.

The stress-strain curves of CFRP and adhesive were obtained from the experiment of related materials, as shown in Fig. 15(a). During the test, most of the specimens occurred completely debonding failure or mixed failure, and the CFRP sheets were far from reaching its yield strength and thus it can be simplified as a linear manner as initially assumed in Fig. 4(a).

**Table 5**
Comparison between calculated and tested results.

| Specimen number | $P_y$(kN) | $P_u$(kN) | $\bar{P}_y$ (kN) | $P/\bar{P}_y$ |
|---|---|---|---|---|
| S-0-0 | 5.3 | 14.25 | 6.13 | 0.86 |
| S-A-1 | 5.3 | 7.38 | 6.18 | 0.86 |
| S-A-2 | 5.3 | 13.14 | 6.09 | 0.89 |
| S-A-3 | 5.3 | 13.81 | 6.17 | 0.86 |
| S-A-4 | 5.3 | 14.05 | 6.38 | 0.83 |
| S-B-1 | 3.92 | 13.06 | 6.21 | 0.63 |
| S-B-2 | 6.59 | 19.03 | 6.55 | 1.01 |
| S-C-1 | 7.60 | 24.49 | 6.60 | 1.15 |
| S-C-2 | 9.54 | 25.57 | 6.36 | 1.50 |
| S-D-1 | 5.3 | 16.54 | 6.53 | 0.81 |
| S-D-2 | 5.3 | 16.97 | 6.41 | 0.83 |

During the test as shown in Fig. 15(b), the adhesive layer was in the elastic force stage at the beginning. When the stress reaches the yield stress $\tau_y$, the adhesive layer entered the elastoplastic stage. By the torsion test of the casted adhesive, it was known that the shear stress $\tau_y$ of the plastic stage remained unchanged, and there was a yielding platform during the plastic development, where the shear load remained unchanged with the increasing of elongation. When the shear strain $\gamma$ of adhesive layer reached the ultimate shear strain $\gamma_u$, the adhesive layer occurred debonding failure. Therefore, the shear stress-strain relationship can be simplified to an ideal elastic-plastic curve, as shown in Fig. 4(b), where $\gamma_y = 2.65$and $\gamma_u = 3.25$.

## 5. Further parametric study and discussions of bond strength

### 5.1. Effects of critical design parameters on bonding shear stress

The analytical model in Section 2 was used to determine the design parameters affecting the bond shear stress and its distribution, such as the material strength, thickness, bonding width, elastic modulus, and Poisson ratio.

The shear stress of the adhesive layer in the elastic stage can be obtained by.

$$\tau(x)=\frac{G_a\gamma_y}{sinh(\beta l)}sinh[\beta(l-x)], \quad 0 \le x \le l \tag{15}$$

where $\gamma_y$is the yield strain of the adhesive layer, and determined by the material properties of the adhesive layer; $G_a$is the shear modulus of the adhesive layer, defined by.

$$G_a = \frac{E_a}{2(1+\upsilon_a)} \tag{16}$$

By the force balance in Fig. 5, the shear stress between the CFRP sheet and stainless steel plate can be obtained, and the calculation formula is as follows:

$$\tau_i = \frac{(\varepsilon_i - \varepsilon_{i-1})\, E_c t_c}{\Delta l_i} \tag{17}$$

In Eq. (17), $\tau_i$ represents the shear stress at the midpoint between the measuring point $i$ and $i-1$; $\varepsilon_i$ and $\varepsilon_{i-1}$ are the strain of CFRP sheets at the point $i$ and $i-1$, respectively; $\Delta l_i$ is the distance between the point $i$ and $i-1$.

The strain gauges have a limited measuring length, which makes it difficult to densely arrange the strain gauges in a certain range near the beam end. Therefore, it is difficult to collect the strain data at the position near the beam end. Therefore, the shear stress distribution curve was captured only when specimens approximately reach the plastic critical stage at the plastic critical load of $0.40P_u$.

The shear stress obtained by the Eqs. (15) and (17) is shown in Fig. 16, including the shear stress distribution of the results predicted by the proposed model, and the test results under different bonding length($l$), the different bonding width($b_c$), the different layer($n$), and the different length of the extra transverse bonded CFRP sheets($l_a$).

From Fig. 16(a)–(d), it is known that the bonding shear stress tested shows good agreement with that of the theoretical calculation. Meanwhile, the influence of the bonding length and the length of the extra transverse bonded CFRP sheets on the shear stress distribution in the elastic stage is very less. The three distribution curves of shear stress with different bonding width are almost coincident in Fig. 16(b), which shows that the parameter ($b_c$) has little influence on the distribution of shear stress in the elastic phase. In the area near the seam end, there is a severe stress concentration, and the peak of the curve appears at the seam end. Meanwhile, the shear stress distribution far from the seam end is almost zero. All the above mentioned is consistent with the internal force analysis results of the elastic stage.

From Fig. 16(c), it is shown that when the layer number of CFRP sheet is one or two, the tested results are close to the theoretical

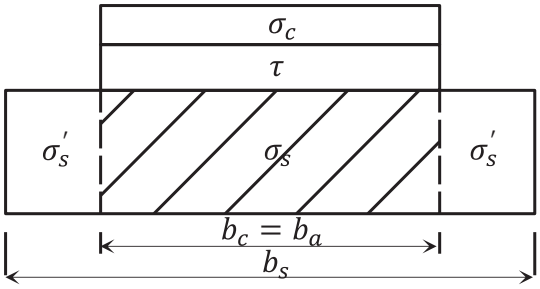


**Fig. 17.** Force profile diagram of composite component.

calculated results, while the tested one is slightly larger than that of calculated at three layers. However, their distribution rules are consistent. This is mainly because the layer number is less, the tensile strain in CFRP sheets can be regarded as uniform distribution (i.e., the surface strain can represent the internal tensile strain). When the layer number is more, the internal tensile strain is no longer evenly distributed, and the different degrees of slippage between the CFRP sheets and the adhesive layer resulted that the shear stress between the measured points is higher than that of theoretical value.

### 5.2. Critical capacity prediction associated to bond shear stress

When the shear stress reaches the maximum($\tau_y$), there is a critical load ($P_y$=$\beta\gamma_y t_a E_C A_C$) defined by Eq. (15). The test results ($\bar{P_y}$) and the results ($P_y$)predicted by the proposed model are as listed in Table 5.

It is shown in Table 5 that when the bonding width is a certain, the actual critical load $\bar{P_y}$ changes very little as the bonding length increasing, i.e., the bonding length has no effect on the stress and strain in the elastic stage. When the bonding width ($b_c$) is 40 mm or 50 mm, the theoretical result is close to the tested one. When the bonding width ($b_c$) is 30 mm, the relative error is larger. This is because in the actual test process, the stainless steel plate is not isotropic. As shown in Fig. 17, although the influence of the bonding width ($b_c$) on the tested results was taken into account in the parameter ($\beta$), the tensile stress ($\sigma$) in the stainless steel plate was not divided into two parts of $\sigma_s$ and $\sigma_s'$ in the force analysis, and the partial stress ($\sigma_s'$) participating in resisting the external load was ignored, which made the calculated result was relatively small. When the bonding width ($b_c$) is similar to the stainless steel plate width($b_s$), the calculated results were in good agreement with that of he tested results. Note that the deviation between the test and predicted results could result from certain uncertainties during the fabrication and tests, such as uneven adhesive layer between multilayer CFRP sheets, fabrication error (the bubble of the adhesive layer in the solidification process), could affect the compactness of the paste.

## 6. Conclusion

This study investigated the bond behavior of CFRP-to-stainless steel plate through both analytical model and experiment. Some conclusions can be drawn as follows.

- By defining four stages, the proposed model could effectively describe the whole load time-history bond behavior of CFRP-to-stainless steel.
- The proposed model by define adhesive layer as an ideal elastic-plastic material, and the CFRP sheet and stainless steel plate as the linear elastic material could be sufficient to predict the bond behavior of CFRP-to-stainless steel, including bond shear stress distribution and crucial load associated to bond strength. The experimental observation revealed that adhesion failure between the adhesion and the CFRP sheets was dominant, and thus confirms the assumption using linear stress-strain relations for the CFRP and stainless steel.
- When the bonding width of CFRP sheets is close to that of the stainless steel plate and the number of CFRP layers is less, the effect of bonding length and length of the extra transverse bonded CFRP on the distribution of shear stress and critical load is less. When the bonding length is sufficient, increasing the number of CFRP layers will influence the distribution of the internal strain of the CFRP sheets, so that the slippage between the CFRP sheets in different layers are not synchronous, which will affect the distribution of shear stress and the critical load.
- When the specimen was in the elastic stage, the stress and strain of the adhesive layer was mainly concentrated near the seam end, and there was little strain far from the seam end. When the load reached the critical status, the plastic zone appeared at the seam end, and the shear stress achieved the maximum. With the continuous expansion of plastic zone, the elastic zone gradually moved away from the seam end. When the plastic zone of the seam end reached the maximum and the elastic zone develops to the farthest, the effective bonding length can be described as $l = le + l_p$, and the shear strain in the plastic zone achieved the yield strain ($\gamma_u$). Hereafter, the adhesive layer cannot resist the external shear load, and the first debonding occurred.
- Due to limitations from assumptions used in the proposed model, there existed deviation between the measurement and the prediction at certain points. The prediction model could be further modified to account for more widespread real-world application.

## Acknowledgements

This study was generously funded by the National Natural Science Foundation of China (Grant No. 51768044), Xihua University key fund (Grant No. z1120634) and Xihua University graduate innovation fund (Grant No. ycjj2017189). The first author also appreciated the support from North Dakota State University during the period of the time when he worked as a visiting scholar. The authors are most grateful to these organizations for their valuable support.

## References

[1] SEI/ASCE-8-02 Specification for the design of cold formed stainless steel structural members. Virginia, USA: American Society of Civil Engineers; 2002.
[2] EC3 Eurocode 3: Design of Steel Structures-Part 1.4: General rules-supplementary rule for stainless steels. European Committee for Standardization, ENV 1993-1-4, CEN, Brussels; 2006.
[3] AS/NZS Australian/New Zealand Standard: Cold-formed stainless steel structures. Sydney, Australia; 2001.
[4] Meier U. Strengthening of structures using carbon fibre/epoxy composites. Constr Build Mater 1995;9(6):341–51.
[5] Edberg W, Mertz D, Gillespie JJ. Rehabilitation of steel beams using composite materials. Proceedings of the materials engineering conference, materials for the new millennium. New York, NY: ASCE; 1996.
[6] Fakharifar M, Sharbatdar M, Lin Z, Dalvand A, Sivandi-Pour A, Chen G. Seismic performance and global ductility of RC frames with retrofitted joints by CFRP laminates. Earthquake Eng Eng Vibration 2014;13:59–73.
[7] Alemdar F, Gangel R, Matamoros A, et al. Use of CFRP overlays to repair fatigue damage in steel plates under tension loading. J Compos Constr 2015;18(4):2537–47.
[8] Kim YJ, Brunell G. Interaction between CFRP-repair and initial damage of wide-flange steel beams subjected to three-point bending. Compos Struct 2011;93(8):1986–96.
[9] Zhao XL, Zhang L. State-of-the-art review on FRP strengthened steel structures. Steel Constr 2008;29(8):1808–23.
[10] Yu T, Fernando D, Teng JG, Zhao XL. Experimental study on CFRP-to-steel bonded interfaces. Compos B Eng 2012;43(5):2279–89.
[11] Damatty AAE, Abushagur M. Testing and modeling of shear and peel behavior for bonded steel/FRP connections. Thin-Walled Struct 2003;41(11):987–1003.
[12] Teng JG, Yu T, Fernando D. Strengthening of steel structures with fiber-reinforced polymer composites. J Constr Steel Res 2012;78(6):131–43.
[13] Nozaka K, Shield CK, Hajjar JF. Design of a test specimen to assess the effective bond length of carbon fiber-reinforced polymer strips bonded to fatigued steel bridge girders. J Compos Constr 2005;9(4):304–12.
[14] Zeng J, Gao W, Liu F. Interfacial behavior and debonding failures of full-scale CFRP-strengthened H-section steel beams. Compos Struct 2018;201(1):540–52.
[15] Chandrathilaka E, Gamage J, Fawzia S. Mechanical characterization of CFRP/steel

bond cured and tested at elevated temperature. Compos Struct 2019;207:471–7.
[16] Yu Q, Gao R, Gu X, Zhao X, Chen T. Bond behavior of CFRP-steel double-lap joints exposed to marine atmosphere and fatigue loading. Eng Struct 2018;175(15):76–85.
[17] Yang Y, Biscaia H, Chastre C, Silva M. Bond characteristics of CFRP-to-steel joints. J Constr Steel Res 2017;138:401–19.
[18] Wang H, Wu G. Bond-slip models for CFRP plates externally bonded to steel substrates. Compos Struct 2018;184(15):1204–14.
[19] Wu ZS, Yuan H, Niu HD. Stress transfer and fracture propagation in different kinds of adhesive joints. J Struct Eng ASCE 2002;128(5):562–73.
[20] Xia SH, Teng JG. Behavior of FRP-to-steel bonded joints Hong Kong, China Proceedings of the international symposium on bond behavior of FRP in structures (BBFS). 2005.
[21] Fawzia S, Zhao XL, Al-Mahaidi R, et al. Preliminary bond-slip model for CFRP sheets bonded to steel plates Florida USA Third international conference on frp composites in civil engineering (CICE) Miami. 2006.
[22] Fawzia S, Zhao XL, Al-Mahaidi R. Bond–slip models for double strap joints strengthened by CFRP. Compos Struct 2010;92(9):2137–45.
[23] Kim YJ, Harries KA. Modeling of steel beams strengthened with CFRP strips including bond-slip properties. Adv Frp Compos Civ Eng 2011:873–6.
[24] Dehghani E, Daneshjoo F, Aghakouchak AA, et al. A new bond-slip model for adhesive in CFRP–steel composite systems. Eng Struct 2012;34(1):447–54.
[25] Yuan H, Teng JG, Seracino R, et al. Full-range behavior of FRP-to-concrete bonded joints. Eng Struct 2004;26(5):553–65.
[26] Youssef MA. Analytical prediction of the linear and nonlinear behavior of steel beams rehabilitated using FRP sheets. Eng Struct 2006;28(6):903–11.
[27] Lam ACC, Yam MCH, Cheng JJR, et al. Study of stress intensity factor of a cracked steel plate with a single-side CFRP composite patching. J Compos Constr 2010;14(6):791–803.
[28] Bocciarelli M, Colombi P, Fava G, et al. Prediction of debonding strength of tensile steel/CFRP joints using fracture mechanics and stress based criteria. Eng Fract Mech 2009;76(2):299–313.